DEVELOPMENT OF A ROBOTIC SIMULATION PLATFORM FOR SPACECRAFT PROXIMITY OPERATIONS AND CONTACT DYNAMICS EXPERIMENTS

A Thesis

by

AUSTIN BREIEN PROBE

Submitted to the Office of Graduate and Professional Studies of
Texas A&M University
in partial fulfillment of the requirements for the degree of

MASTER OF SCIENCE

Chair of Committee,	John L. Junkins
Committee Members,	John E. Hurtado
	Alan Palazzolo
Head of Department,	Rodney D. W. Bowersox

December 2013

Major Subject: Aerospace Engineering

ABSTRACT

A major challenge facing the introduction of new technologies and techniques in space flight is the high cost required to raise the Technological Readiness Level (TRL) prior to flight. This is a result of the cost and scarcity of developmental launch opportunities for verification and validation. A ground facility with the capability for six degree-of-freedom robotic spacecraft emulation that enables laboratory-based hardware-in-the-loop experiments is desired, to allow for the simulation of space-based operations for almost any mission. Such a facility would enable experiments that can be used pre-flight to reduce development cost and ensure the functionality of sensor suites with guidance, navigation, and control systems. However, a major shortfall of most robotic motion emulation systems is the inability to simulate proximity operations involving contact dynamics, due to their methods of actuation and required dynamic response time. To provide this capability at the Texas A&M Land Air and Space Robotics (LASR) Lab, a novel low-cost robotic platform called the Suspended Target Emulation Pendulum (STEP) was developed. This thesis details the design, system dynamics, simulation, and control of the STEP system, and presents experimental results from an initial prototype.

To Shannon, who is amazing,

and my parents who made this possible.

ACKNOWLEDGEMENTS

Thanks to Kurt Cavalieri, Brent Macomber, and Clark Moody at LASR and Dr. Jeremy Davis and James Doebbler at VectorNav Technologies. I would also like to extend my sincere thanks to Dr. John Junkins and Dr. John Hurtado for their advice and mentorship.

This work was supported by NASA Johnson Space Center under the Small Business Technology Transfer (STTR) program, and we would specifically like to thank Dr. J.-C. Liou, our technical adviser, for his support.

TABLE OF CONTENTS

Page

CHAPTER Page

LIST OF FIGURES

FIGURE Page

LIST OF TABLES

CHAPTER I

INTRODUCTION

I.A. Motivation

The major objective of the Land, Air, and Space Robotics (LASR) Laboratory at Texas A&M University is to allow for hardware-in-the-loop experiments simulating the realistic performance of aerospace systems for the evaluation of Guidance, Navigation, and Control (GNC) techniques.

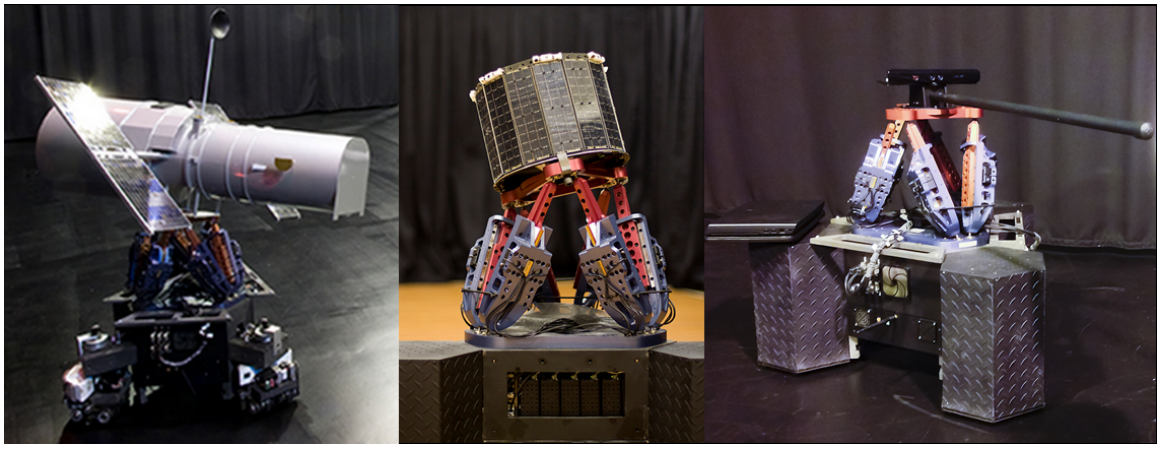

Figure I.1: HOMER Mounted with Several Experimental Payloads

This objective is achieved using a combination of the Holonomic Omnidirectional Motion Emulation Robot (HOMER) and several inertial sensing systems. HOMER, shown in several configurations in Figure I.1, was designed to physically emulate

the six degree-of-freedom (6-DOF) motion of aerospace systems in a laboratory work-space to reproduce the motion of a desired vehicle based on a computational simulation with high fidelity. [1] Two independent inertial measurement systems, specifically Vicon™and Nikon iGPS™, provide 6-DOF position information for rigid bodies within the lab space with millimeter and small fraction of degree level accuracy. By outfitting HOMER with the sensor payloads of some spacecraft system it becomes possible to command HOMER as if it were that system and have it reproduce the dynamics that system would experience. Measuring this experiment with the inertial sensing systems provides an excellent approximation of the "truth" that can be used to evaluate the GNC system.

However, there are two major drawbacks of this system that make it incapable of preforming proximity operations experiments where contact dynamics are involved. The first is the actuation used by HOMER. HOMER consists of a Stewart platform driven by piezoelectric linear motors on top of a base moved by active castors. The bandwidth of these actuators is not high enough to simulate contact dynamics accurately. Secondly, neither of the systems is capable of slip and the Stewart platform actuators will simply shutdown if overloaded during an impact. Additionally, even if the actuators were capable of the necessary bandwidth it is impossible with current sensors to measure the forces from an impact that occurs during an experiment and dynamically compute the response that the real system would experience in real-time with sufficient precision. Unfortunately, contact dynamics is a critical issue for many important space missions, such as orbital-debris capture, rendezvous and docking, on-orbit refueling or service, and scientific small-body missions (e.g.

asteroid capture). These limitations motivated the development of the Suspended Target Emulation Pendulum (STEP).

I.B. Suspended Target Emulation Pendulum Concept

The goal of the Suspended Target Emulation Pendulum is to construct a 5-DOF, pendulum-based, motion simulator to which the mock target vehicles will be attached. The target vehicle is suspended from a long spherical pendulum with its pivot point actively positioned by a 2-axis gantry. The idea is to actuate the gantry moving the pivot point to accurately "chase" the mass center of the target vehicle such that the pendulum remains near vertical and the target maintains "space like" motion in a horizontal plane. The pendulum is also designed to rotate to simulate the case of a body in pure spin. The target vehicle is suspended by a universal joint at, or very near, its center of gravity, allowing for a small range of motion for the target in the two rotational degrees of freedom orthogonal to the pendulum. A detailed view of the STEP system concept is provided in Figure I.2

This system is designed for use in conjunction with another robotic simulation system like HOMER to simulate a contact event. An early concept of a possible experiment is shown in Figure I.3. The second robotic system will impact the STEP target vehicle and the ability of the pendulum to swing will allow for instantaneous motion, and because the pendulum is long enough that the motion will be within the linear range of the small angle assumptions and therefore small initial motions will be similar to what would be experienced in a space environment. The gantry can then be used to move the pivot point and keep the pendulum within this sweet-

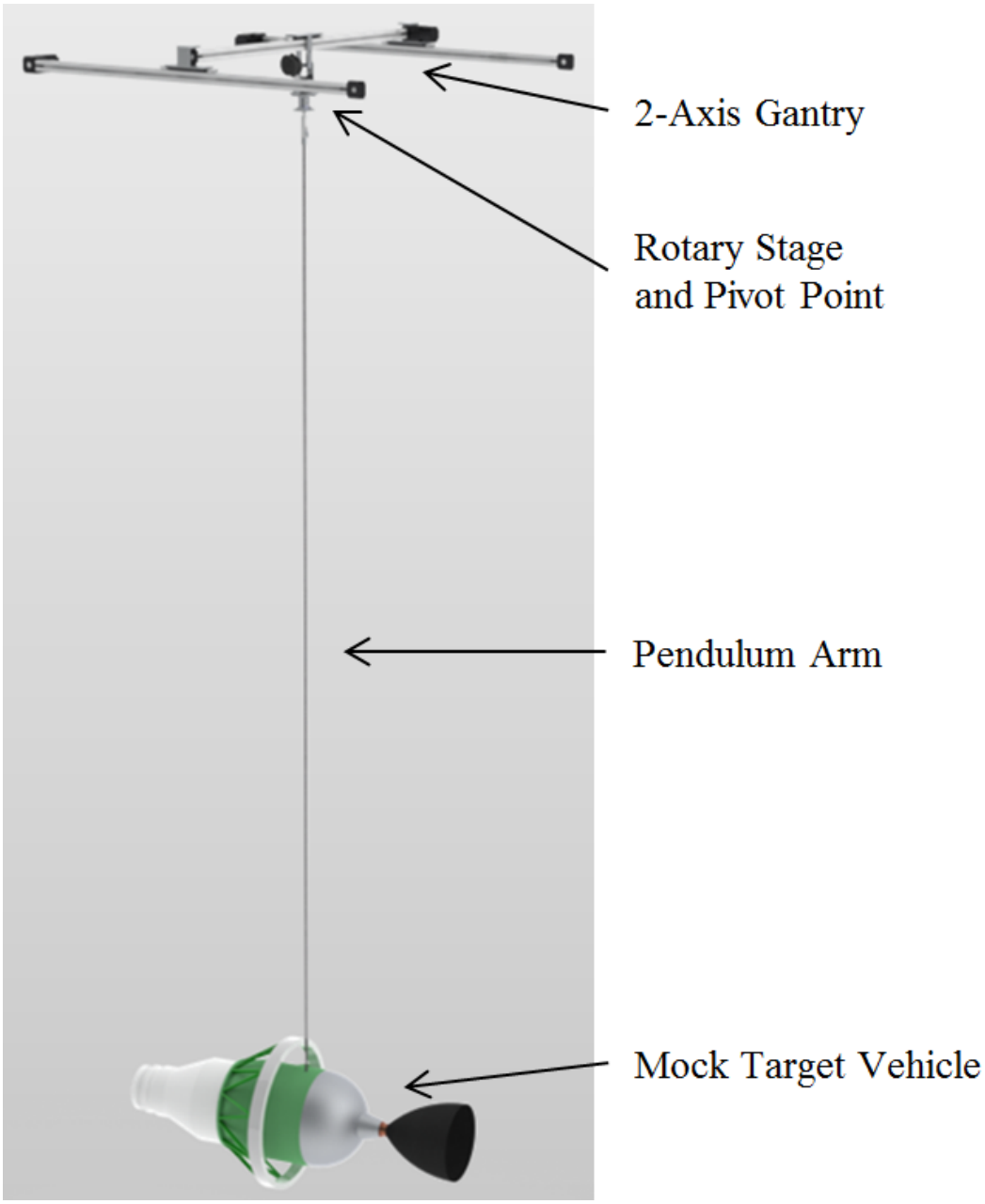

Figure I.2: STEP System Concept

spot, increasing the range where the "space like" motion is possible. The gantry will maintain the required motion until it reaches the edge of the usable work space at which point the gantry will be used to stabilize the target, and bring it to rest. When the STEP system is stabilizing, the relative motion of the two vehicles can be approximately transferred to the other robotic platform allowing the experiment to continue. This thesis details the design of an initial version of the STEP system, development of a system simulation, the design of a system controller, and finally the construction and implementation of system prototypes.

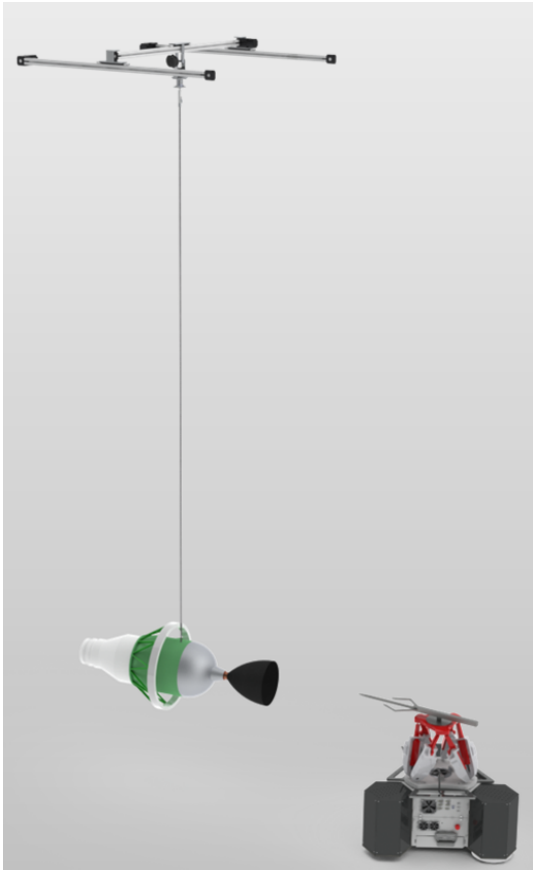

Figure I.3: Early STEP System Concept with HOMER

CHAPTER II

SYSTEM DYNAMICS

To understand the STEP system dynamics Lagrange's Equations were used to derive equations of motion. [2] [3] In this derivation the angular rates and their derivatives are the major quantities of interest and it was assumed that the gantry position and its derivatives were specified as a result of the system control.

II.A. One Dimensional Case

Initially the system dynamical model was derived for a one dimensional gantry with only a singular angular degree of freedom. In this case, illustrated in figure II.1 x represents the displacement along the gantry, theta is the angular displacement from the vertical, l is the length of the pendulum, and m is the mass of the object suspended at the base of the pendulum.

The inertial position vector(2.1) can be simply calculated from the system geometry.

$$\vec{P} = \begin{pmatrix} l\sin(\theta(t)) + x(t) \\ 0 \\ -l\cos(\theta(t)) \end{pmatrix} \tag{2.1}$$

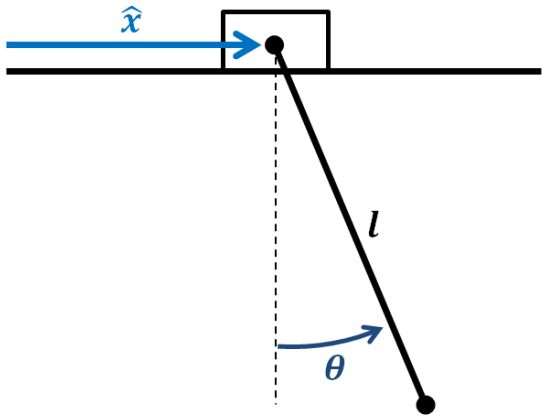

Figure II.1: One Dimensional Case Coordinate System

The inertial velocity vector(2.2) can be obtained with simple differentiation.

$$\vec{V} = \dot{\vec{P}} = \begin{pmatrix} l\dot{\theta}(t)\cos(\theta(t)) + \dot{x}(t) \\ 0 \\ l\dot{\theta}(t)\sin(\theta(t)) \end{pmatrix} \tag{2.2}$$

The kinetic energy of the system(2.3) is half the square of the inertial velocity (2.2) time the mass.

$$T = \frac{1}{2}m\left(l^2\dot{\theta}(t)^2 + 2l\dot{\theta}(t)\cos(\theta(t))\dot{x}(t) + \dot{x}(t)^2\right) \tag{2.3}$$

The potential energy of the system (2.4) is the gravitational potential multiplied by the mass and the z component of the inertial position (2.1).

$$U = -mgP_Z = glm\cos(\theta(t)) \tag{2.4}$$

The system Lagrangian can be trivially calculated from the kinetic and potential energy(2.3-2.4).

$$L = T - U = \frac{1}{2}m\left(l^2\dot{\theta}(t)^2 + 2l\dot{\theta}(t)\cos(\theta(t))\dot{x}(t) + \dot{x}(t)^2\right) - glm\cos(\theta(t)) \tag{2.5}$$

Plugging the Lagrangian (2.5) into the virtually non-working form of the Lagrange Equation (2.6), a system equation of motion (2.7) can be found.

$$\frac{d\left({}^{dL}/_{d\dot{\theta}}\right)}{dt} - \frac{dL}{d\theta} = 0 \tag{2.6}$$

$$0 = lm\left(-g\sin(\theta(t)) + l\ddot{\theta} + \cos(\theta(t))\ddot{x}(t)\right) \tag{2.7}$$

Solving for $\ddot{\theta}$ provides the angular acceleration of the pendulum (2.8).

$$\ddot{\theta}(t) = \frac{g\sin(\theta(t)) - \cos(\theta(t))\ddot{x}(t)}{l} \tag{2.8}$$

II.B. Full System Dynamics

The full system dynamics were derived using the same methodology as the single degree of freedom system, but with the addition of a second dimension for the gantry and an additional angular degree of freedom. In the full system case, illustrated in Figure II.2 x and y represent the position in the gantry plane, θ and ϕ are the angular displacements from the vertical that move the pendulum in the positive x and y direction respectively, l is the length of the pendulum, and m is the mass of the object suspended at the base of the pendulum. This setup actually results in θ

being a negative angle in a standard right-handed coordinate system, however it was chosen as a matter on convenience.

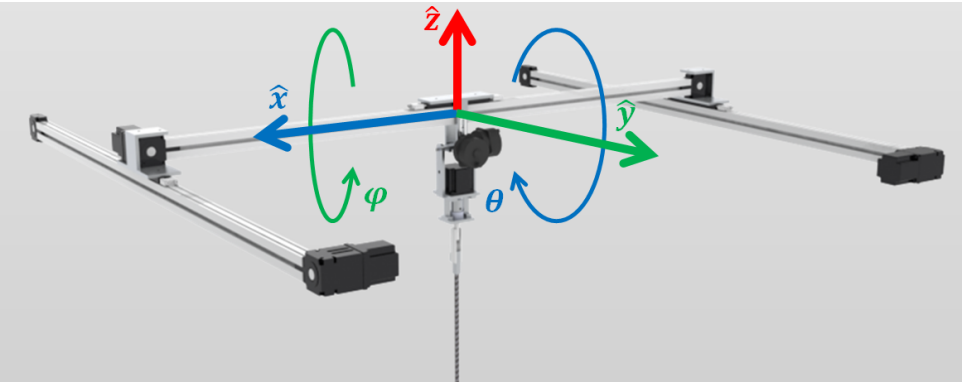

Figure II.2: Full System Coordinate Frame

The position vector of the full system can be found combining the inertial gantry position with the body frame position of the pendulum rotated into the inertial frame with a direction cosin matrix from a 1-2 Euler rotation sequence through $-\theta$ and ϕ.

$$\vec{P} = \begin{pmatrix} x \\ y \\ 0 \end{pmatrix}_N + DCM(-\theta, \phi) * \begin{pmatrix} 0 \\ 0 \\ -l \end{pmatrix}_B \tag{2.9}$$

where

$$DCM(-\theta, \phi) = \begin{bmatrix} \cos(\theta(t)) & 0 & \sin(\theta(t)) \\ -\sin(\theta(t))\sin(\phi(t)) & \cos(\phi(t)) & \cos(\theta(t))\sin(\phi(t)) \\ -\cos(\phi(t))\sin(\theta(t)) & -\sin(\phi(t)) & \cos(\theta(t))\cos(\phi(t)) \end{bmatrix} \tag{2.10}$$

The resulting inertial position vector:

$$\vec{P} = \begin{pmatrix} x(t) - l\sin(\theta(t)) \\ y(t) - l\cos(\theta(t))\sin(\phi(t)) \\ -l\cos(\theta(t))\cos(\phi(t)) \end{pmatrix} \tag{2.11}$$

The inertial velocity vector:

$$\vec{V} = \begin{pmatrix} \dot{x} - l\dot{\theta}\cos(\theta(t)) \\ l\dot{\theta}\sin(\theta(t))\sin(\phi(t)) - l\cos(\theta(t))\dot{\phi}\cos(\phi(t)) + \dot{y} \\ l\dot{\theta}\sin(\theta(t))\cos(\phi(t)) + l\cos(\theta(t))\dot{\phi}\sin(\phi(t)) \end{pmatrix} \tag{2.12}$$

The kinetic energy:

$$\begin{aligned} T =& \frac{1}{2}m\Big[\Big(l\dot{\theta}\sin(\theta(t))\cos(\phi(t)) + l\cos(\theta(t))\dot{\phi}\sin(\phi(t))\Big)^2 \\ &+ \Big(\dot{x} - l\dot{\theta}\cos(\theta(t))\Big)^2 + \Big(l\dot{\theta}\sin(\theta(t))\sin(\phi(t)) \\ &-l\cos(\theta(t))\dot{\phi}\cos(\phi(t)) + \dot{y}\Big)^2\Big] \end{aligned} \tag{2.13}$$

The potential energy:

$$U = -mgP_Z = glm\cos(\theta(t))\cos(\phi(t)) \tag{2.14}$$

The Lagrangian:

$$\begin{aligned} L =& \frac{1}{2}m\Big[-2gl\cos(\theta(t))\cos(\phi(t)) + \Big(l\dot{\theta}\sin(\theta(t))\cos(\phi(t)) \\ &+ +l\cos(\theta(t))\dot{\phi}\sin(\phi(t))\Big)^2 + \Big(\dot{x} - l\dot{\theta}\cos(\theta(t))\Big)^2 \\ &+ \Big(l\dot{\theta}\sin(\theta(t))\sin(\phi(t)) - l\cos(\theta(t))\dot{\phi}\cos(\phi(t)) + \dot{y}\Big)^2\Big] \end{aligned} \tag{2.15}$$

The virtually non-working Lagrange equation for θ:

$$\frac{d\left({}^{dL}/_{d\dot{\theta}}\right)}{dt} - \frac{dL}{d\theta} = 0 \tag{2.16}$$

$$\begin{aligned} 0 = lm \Big(& -g\sin(\theta(t))\cos(\phi(t)) + l\ddot{\theta} + l\sin(\theta(t))\cos(\theta(t))\dot{\phi}^2 \\ & - \cos(\theta(t))\ddot{x} + \sin(\theta(t))\ddot{y}\sin(\phi(t))) \end{aligned} \tag{2.17}$$

The virtually non-working Lagrange equation for ϕ:

$$\frac{d\left({}^{dL}/_{d\dot{\phi}}\right)}{dt} - \frac{dL}{d\phi} = 0 \tag{2.18}$$

$$\begin{aligned} 0 = -lm\cos(\theta(t)) \Big(& g\sin(\phi(t)) + 2l\dot{\theta}\sin(\theta(t))\dot{\phi} \\ & -l\cos(\theta(t))\ddot{phi} + \ddot{y}\cos(\phi(t)) \Big) \end{aligned} \tag{2.19}$$

Equations 2.17 and 2.19 can be combined into a system and solved for $\ddot{\theta}(t)$ and $\ddot{\phi}(t)$:

$$\ddot{\theta} = \frac{\sin(\theta(t))\left(g\cos(\phi(t)) - \ddot{y}\sin(\phi(t))\right) - l\sin(\theta(t))\cos(\theta(t))\dot{\phi}^2 + \cos(\theta(t))\ddot{x}}{l} \tag{2.20}$$

$$\ddot{\phi} = \frac{\sec(\theta(t))\left(g\sin(\phi(t)) + 2l\dot{\theta}\sin(\theta(t))\dot{\phi} + \ddot{y}\cos(\phi(t))\right)}{l} \tag{2.21}$$

CHAPTER III

DESIGN

There are 4 design requirements and 3 design goals for the STEP system:

1. Requirements
    (a) Operate with a 50±5 kilogram target
    (b) Greater than 1.5 m work-space
    (c) Run with a 0.25 meters per second velocity
    (d) Spin at 30 ° per second
2. Goals
    (a) Accelerate at 0.5 meters per second squared
    (b) Have millimeter level sensor accuracy
    (c) Be as inexpensive as possible

These requirements and goals were designed by considering typical mission requirements and a qualitative consideration of the available budget.

III.A. Major Component Selection

III.A.1. Actuators

Macron Dynamics™MSA-NBC linear belt driven actuators, show in Figure III.1, were selected for the gantry actuation. The actuator's relevant properties are displayed in Table III.1. [4] While these maximum properties easily exceed the requirements and goals specified the actuators require motors to operate and the quality of the motors will determine weather the maximum velocity and acceleration values can be achieved.

Max Velocity	2.54 m/s
Max Load	45.45 kg
Max Acceleration	$> 45 m/s^2$
Max Travel	1.82 m
Travel Distance per Revolution	0.105 m
Pulley Radius	16.7 mm

Table III.1: MSA-NBC Actuator Properties

III.A.2. Actuator Drive Motors

Automation Direct™STP-MTR-23079 stepper motors, show in Figure III.2, were selected as the system drive motor. Stepper motors were chosen because they offer relatively high torque and good accuracy at a low cost. The STP-MTR-23079 motor has a maximum torque of 1.95 Nm, however the actual torque is dependent on the speed, as shown in Figure III.3. To achieve the design specifications the motor must

Figure III.1: Macron MSA-NBC Linear Actuator*

be able to produce the torque required to accelerate or decelerate a 50 kilogram object at .5 meters per second squared. Figure III.3 shows that torque decreases with speed, therefore the limiting case will be decelerating when at maximum speed. The torque required is calculated from equation 3.2.

$$T_{req} = (m * a_{req}) * r_{pulley} \tag{3.1}$$

$$T_{req} = (50kg * 0.25m/s^2) * 0.0167m = 0.208Nm \tag{3.2}$$

The rotation rate of the motor, in RPM, when the actuator is moving at 0.25 meters per second is given by equation 3.4. The circumference of the pulley(C_{pulley}) is equivalent to the travel distance per revolution of the actuator.

$$R_{motor} = 60\frac{sec}{min} * V_{actuator}/C_{pulley} \tag{3.3}$$

*Image Credit: Macron Dynamics™ [4]

$$R_{motor} = 60\frac{sec}{min} * (0.5m/s)/(0.105m/rev) = 285.7RPM \tag{3.4}$$

According to Figure III.3 at 285 RPM the motor should be able to provide over 1.1 Nm of torque, easily exceeding the torque required. At this level of torque the motor should be able to provide in excess of 1.3 meters per second squared of acceleration to a 50 kilogram target. [5]

Figure III.2: Automation Direct STP-MTR-23079 Stepper Motor*

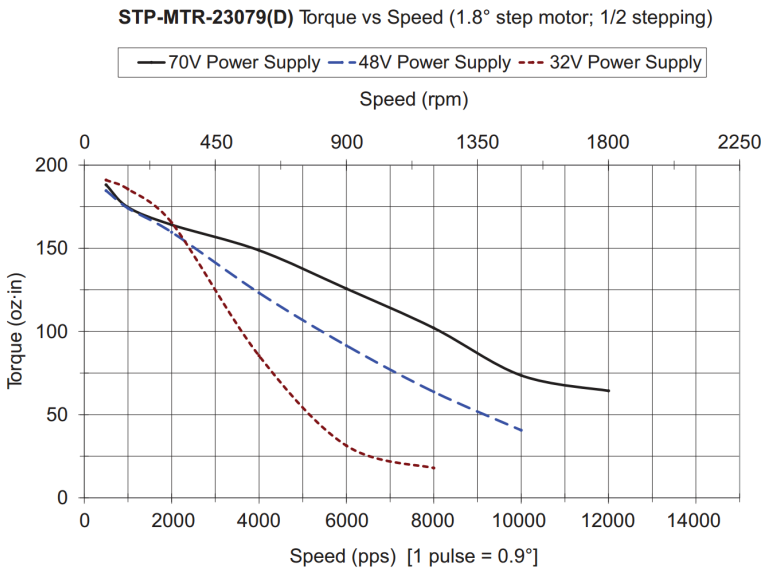

Figure III.3: Available Motor Torque*

*Image Credit: Automation Direct™ [5]

III.A.3. Spin Motor

A Wantai™57BYGH420 stepper motor was selected to drive the pendulum rotation. To meet the design requirement of spinning at 30 ° per second the spin motor only needs to be slightly more powerful than the torque from air resistance and bearing friction, because there is no requirement that it reach its full velocity quickly. This motor was selected for its small form factor and low cost. [6]

III.A.4. Encoders

The encoders selected for use on the STEP system were the US Digital™HBA2 absolute rotary encoder. The specifications of these encoders is shown in Table III.2. [7] The level of positional accuracy based on digital encoder accuracy is given be equation 3.5, where l is the length of the pendulum and $R_{encoder}$ is the digital resolution of the encoder in bits.

Max Acceleration	100000 rad/sec^2
Max Rotation Rate	6000 rpm
Resolution	12 bit
Update Rate	200 Hz

Table III.2: HBA2 Encoder Properties

$$A_{position} = 2 * \pi * l/(2^{R_{encoder}}) \tag{3.5}$$

These encoders provide 12-bit accuracy. Unfortunately with a 4 meter pendulum this only equates to 6.14 millimeters of accuracy, which violates our second design

goal. To achieve millimeter level precision 15-bit accuracy or better would be required. In this case the second design goal was suppressed by the third, because no suitable encoders could be found within the projects budgetary constraints.

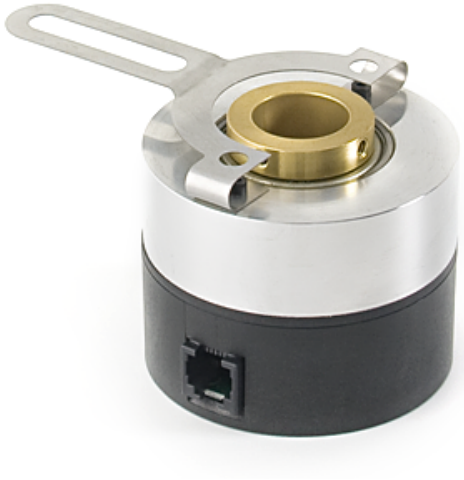

Figure III.4: HBA2 Absolute Rotary Encoder*

*Image Credit: US Digital™ [7]

III.A.5. Attitude Heading Reference System

A VectorNav™VN-100 Attitude Heading Reference System (AHRS) was selected to provide angular rate measurements. This AHRS provides filtered angular rate data at 200 Hz. [8]

Figure III.5: VN-100 Attitude Heading Reference System*

III.B. Final Design

After multiple design iterations and a detailed design review, a final design for the STEP system was completed. The system consists of three MSA-NBC linear actuators, arranged to form the 2-axis gantry, attached to a frame constructed from 80/20 aluminum extrusions. This frame is designed to be mounted to cross support beams in the LASR Laboratory ceiling. The full CAD design for the STEP is shown in Figure III.6.

*Image Credit: VectorNav Technologies™ [8]

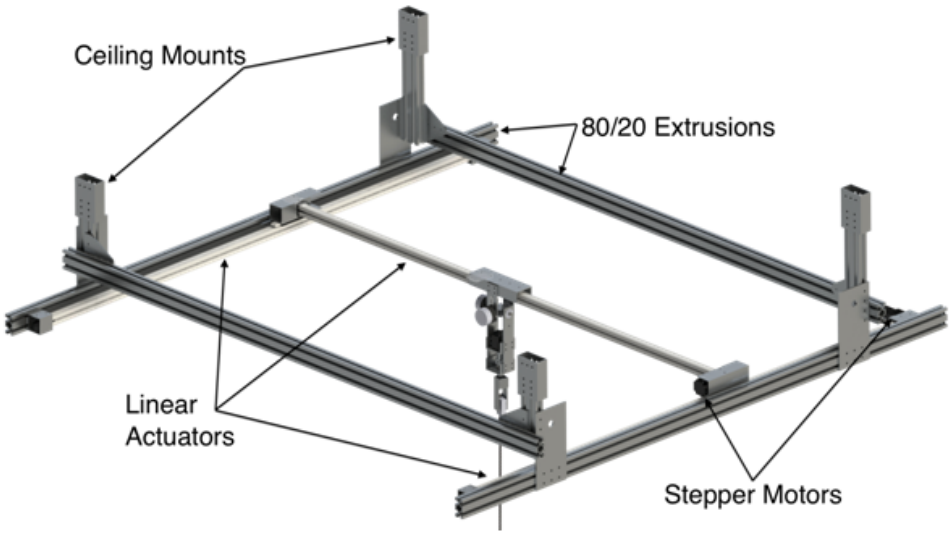

Figure III.6: Dynamic Payload Pendulum CAD Full View

The pivot point of the pendulum is provided via a custom universal joint. The two encoders encoders determine the angle of the pendulum. Laser-cut plexi-glass attachment points are mounted to the linear actuator carts for cable management. A closer look at the universal joint can be seen in Figure III.7.

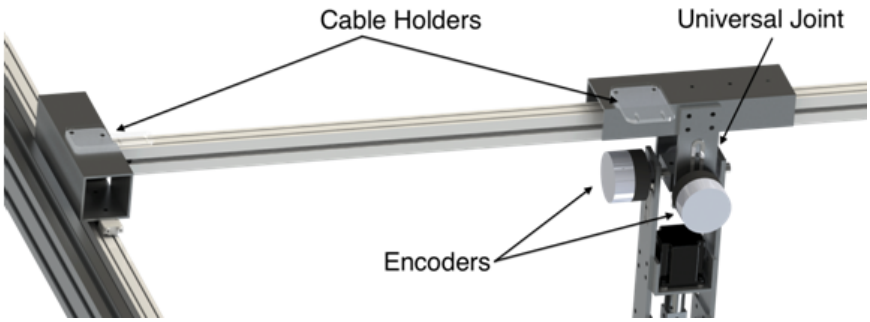

Figure III.7: Dynamic Payload Pendulum CAD Central Actuator View

The pendulum mount is an aluminum frame which holds the spin motor and

provides support using a thrust and roller bearing combination while also allowing rotation. The VN-100 AHRS is attached to the base of the pendulum mount to allow for measurement of the pendulum's angular velocity. The pendulum bar consists of a carbon fiber rod attached to an aluminum hook. This hook mounts into the aluminum housing suspended below the pendulum mount. The hook and housing combination allows the pendulum to be easily mounted during simple tests, but also has alignment holes that allow for the system to be bolted together for precision experiments. A closer look at the pendulum mount design is shown in Figure III.8.

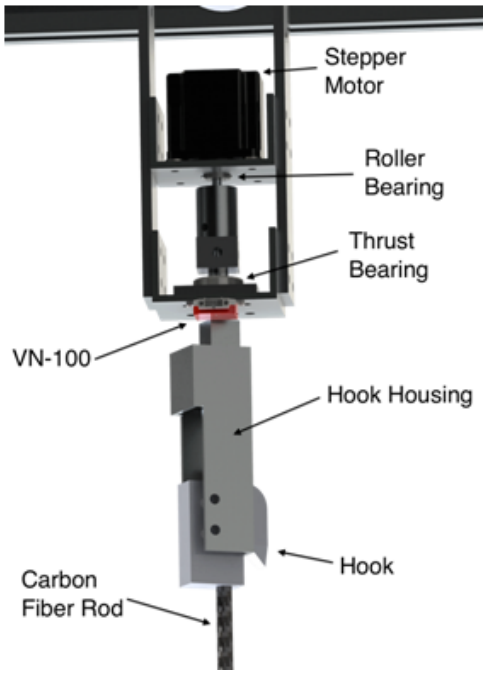

Figure III.8: Dynamic Payload Pendulum CAD Pendulum Mount View

CHAPTER IV

CONTROLLER DEVELOPMENT

The STEP system has has two separate control modes:

Velocity Maintenance: This mode attempts to keep the target moving at the initial velocity imparted from the contact event.

Stabilization: This mode brings the target vehicle to rest once it reaches the edge of the useable gantry space.

One drawback of the stepper motors selected is that they are only capable of being controlled by commanding velocity. This makes the implementation of acceleration based controllers difficult, and as a result the current implementation uses heuristically developed kinematic controllers. [9] The same controllers, although using different gains, were implemented for both one dimensional test-bed and the full system.

IV.A. Velocity Maintenance Controller

The velocity maintenance controller(4.1) is simply a combination of a constant command of the estimated initial target velocity(V_0) and a proportional feed-back controller based on the difference between the estimated goal position($\vec{x}_{est}$) and the current cart position($\vec{x}$) with a control gain(K_P). The initial target velocity

is estimated by averaging the first 10 angular rate readings from the VN-100 ARHS after an impact event and the goal position is estimated by multiplying the initial velocity by the time since the impact event.

$$\vec{U_{VM}} = \vec{V_0} + K_P(\vec{x}_{est} - \vec{x}) \tag{4.1}$$

IV.B. Stabilization Controller

The objective of the stabilization controller is to reduce θ and $\dot{\theta}$ to zero as quickly as possible with minimal travel along the x or y directions. The stabilization controller, shown in equation 4.2 is made up of three different terms. The first is a proportional term feeding back on the angles θ and ϕ $(\vec{\theta})$ and the second is a non-linear proportional term feeding back on the cube of the angles, with gains of K_P and K_{NL} respectively. The final term is proportional term feeding back on the angular rates $(\dot{\vec{\theta}})$ with the gain $K_{\dot{\theta}}$.

$$\vec{U_S} = K_P\vec{\theta} + K_{NL}\vec{\theta}^3 + K_{\dot{\theta}}\dot{\vec{\theta}} \tag{4.2}$$

CHAPTER V

SYSTEM SIMULATION

A Matlab™simulation of the STEP system was developed using the dynamic equations presented in II. The simulation was updated to include time delays, motor models, advanced sensor models, and a damping to represent friction. As a trivial test case, an impulse was applied to the pendulum simulation without control, the response can be seen in Figure V.1. The simulation produced the slightly diminishing oscillatory response you expect from a damped pendulum.

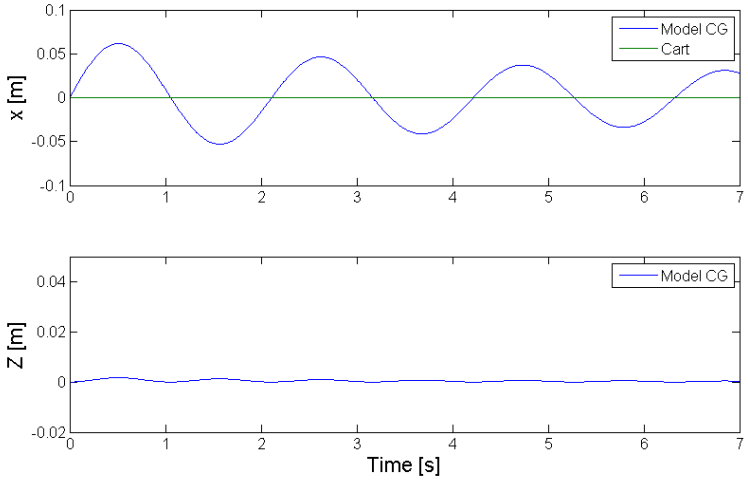

Figure V.1: Pendulum Validation Test

V.A. Dampening Model

Air resistance was assumed to be the dominant factor in the system damping because the pendulum arm is essentially a long cylinder and the target bodies should have relatively low ballistic coefficients. To include damping terms a heuristic damping term was added, shown for θ in Equation 5.1. The value of this term is a dampening constant(C_D) times the square of the angular velocity. [10]

$$\ddot{\theta}_{sim} = \ddot{\theta}_{ideal} - sign(\dot{\theta}) * C_D * \dot{\theta}^2 \tag{5.1}$$

To increase the accuracy of the friction and dampening modeling, a test was preformed on the single degree-of-freedom test-bed (VI.A). Data was taken from this test using the Vicon™motion capture system and compared to the single degree-of-freedom version of the simulation. The results of the friction test, shown in Figure V.2 show that the simulation should provide reliable insight into the response of the actual system.

The system simulation was used to verify the performance of the controllers developed in IV and subsequently tune the various controller gains for both the one dimensional case and the full STEP system.

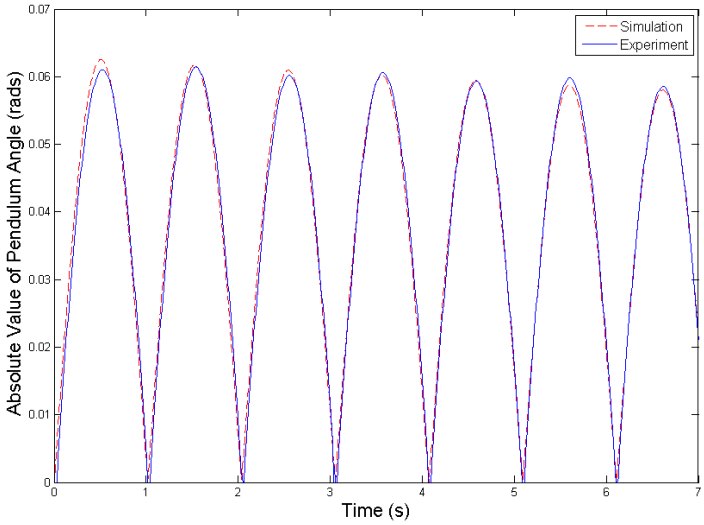

Figure V.2: Dampening Model Validation Test

V.B. One Dimensional Case

The one dimensional case was simulated with the parameters listed in Table V.1. These parameters mirror the physical one dimensional set up as closely as possible.

Pendulum Length	1.10 m
Target Mass	2 kg
Initial Impulse	$0.2m/s$
Max Acceleration	$1m/s^2$
Velocity Maintenance Distance	0.5 m
Control Frequency	100 Hz

Table V.1: One Dimensional Simulation Properties

The velocity maintenance and stabilization controllers were tuned separately, example results are shown in Figures V.3 and V.4, and they were then combined into the full controller setup, where the velocity maintenance controller hands off to the stabilization controller once a limit point on the gantry is reached. The results of the full controller setup are shown in Figure V.5. In Figures V.3 through V.5 the blue line represents the position of the mass at the end of the pendulum, the green line represents the position of the gantry cart, and the dashed red line represents the path of an equivalently massed target moving as it would in space, or the goal state until stabilization.

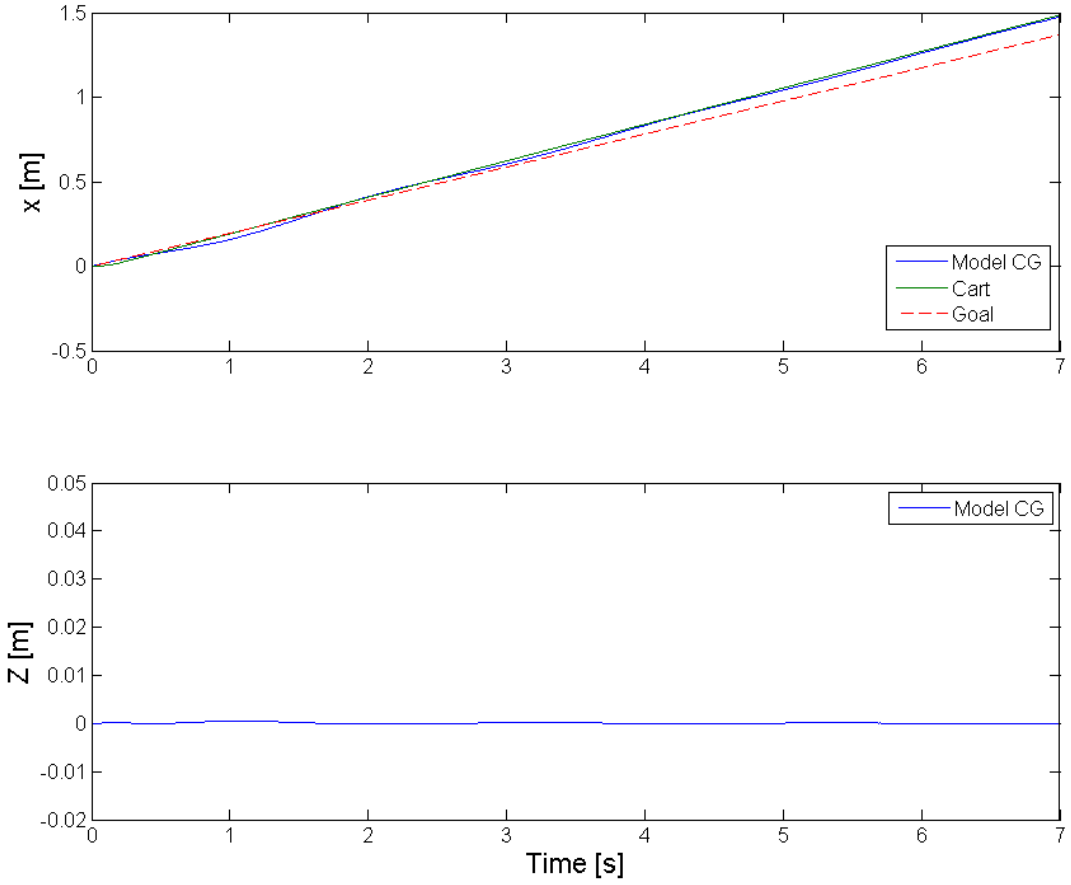

Figure V.3: Simulated One Dimensional Test-Bed with Velocity Maintenance Controller

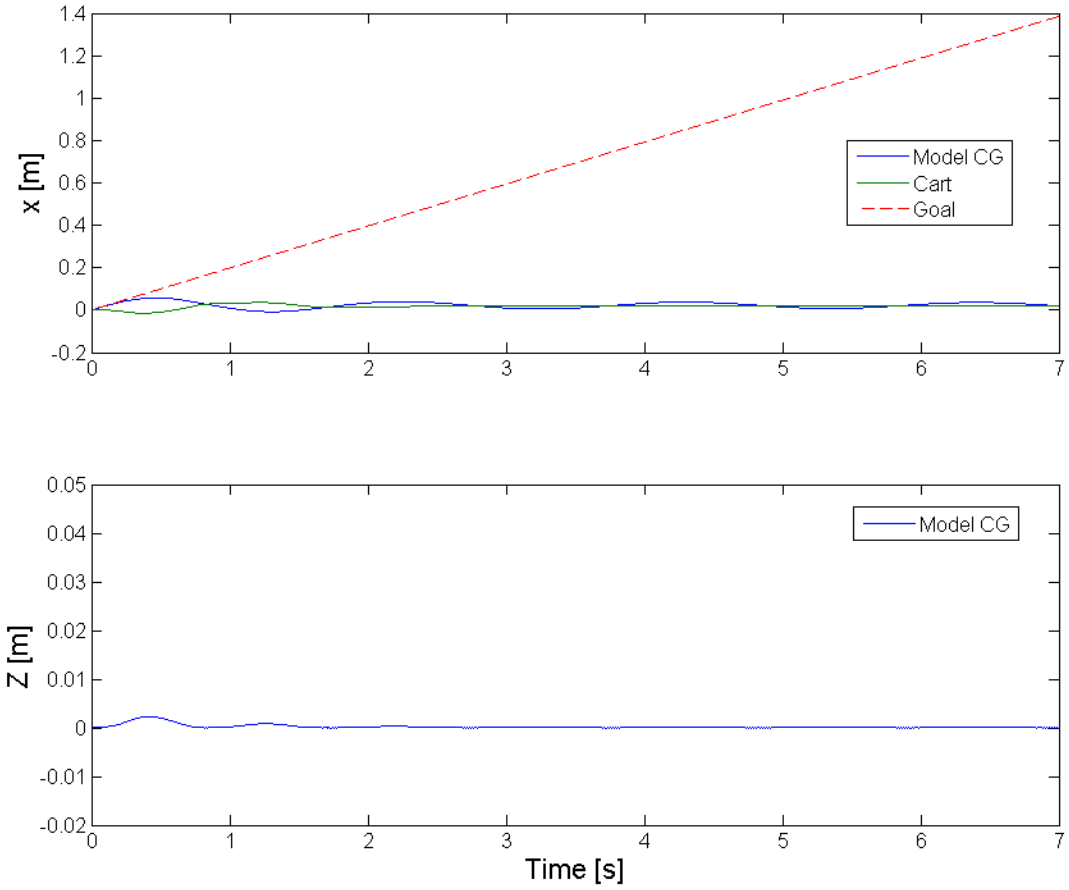

Figure V.4: Simulated One Dimensional Test-Bed with Stabilization Controller

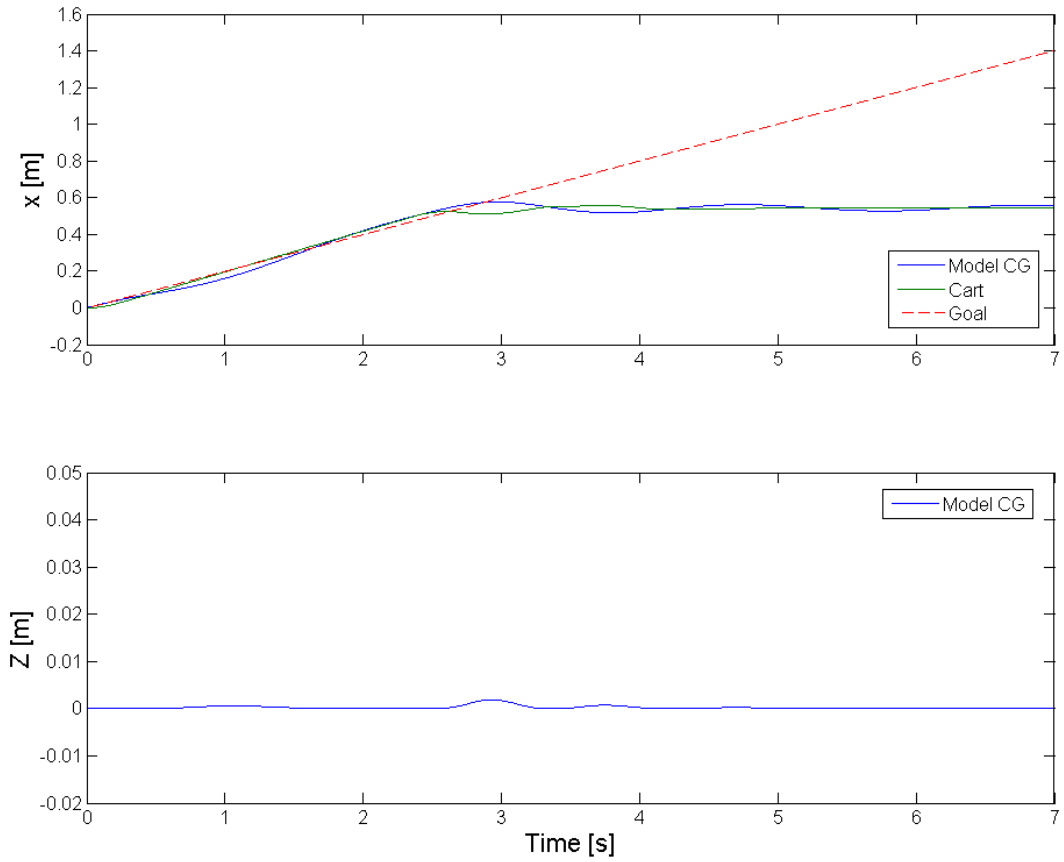

Figure V.5: Simulated One Dimensional Test-Bed with Full Control Implementation

V.C. Full System Simulation

The full STEP system was simulated with the parameters listed in Table V.2.

Pendulum Length	4.0 m
Target Mass	20 kg
Initial Impulse	$0.2m/s$
Initial Impulse Direction Vector	[1 1 0]
Max Acceleration	$0.8m/s^2$
Velocity Maintenance Distance	0.5 m
Control Frequency	100 Hz

Table V.2: Simulated Full STEP Simulation Properties

The process where velocity maintenance and stabilization controllers were tuned separately and integrated into the full controller setup was repeated. Figures V.6 through V.8 show the results. In these plots the blue line represents the position of the mass at the end of the pendulum, the green line represents the position of the gantry cart, and the dashed red line represents the goal state until stabilization.

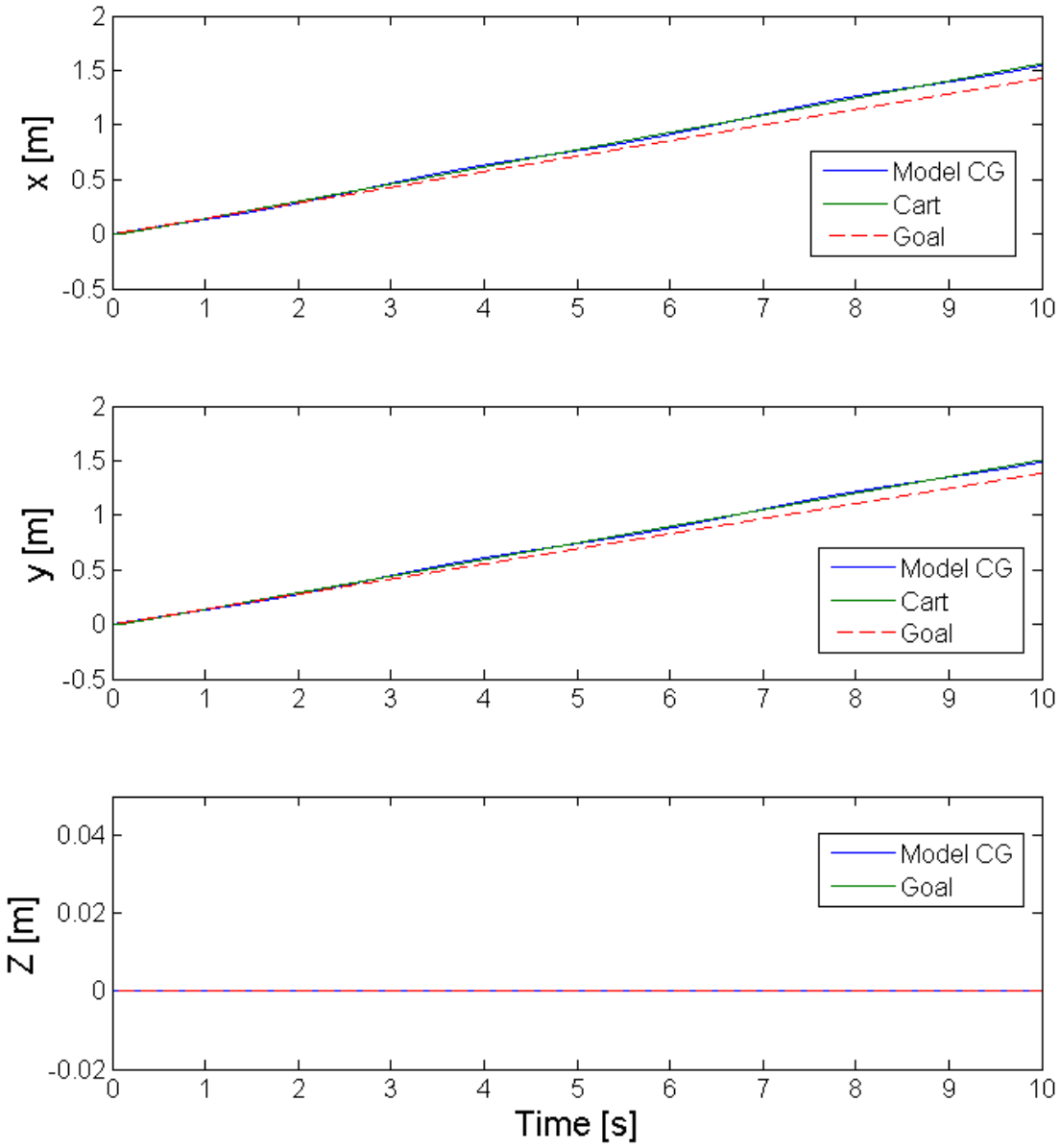

Figure V.6: Simulated STEP with Velocity Maintenance Controller

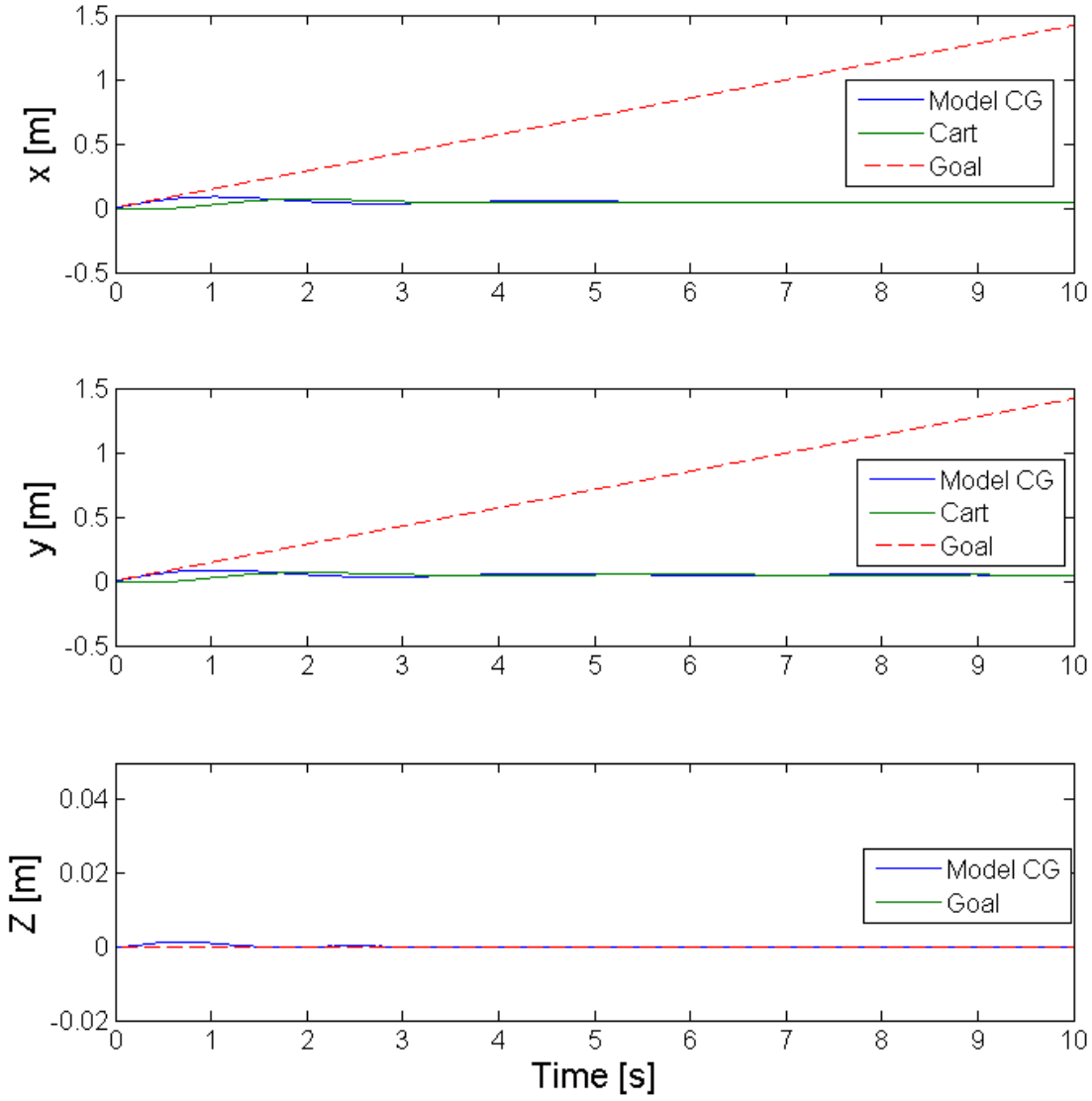

Figure V.7: Simulated STEP with Stabilization Controller

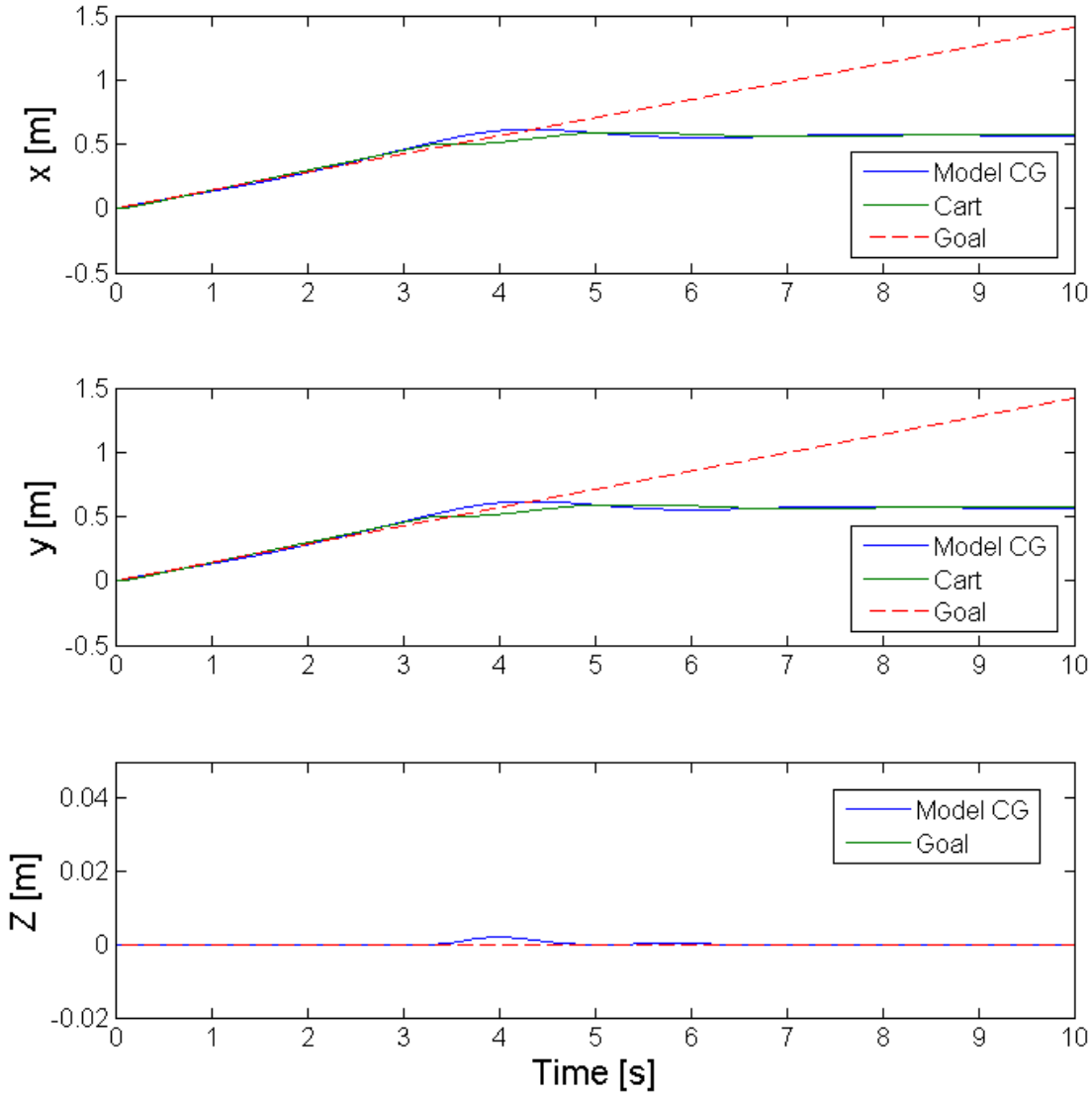

Figure V.8: Simulated STEP with Full Control Implementation

CHAPTER VI

CONSTRUCTION AND IMPLEMENTATION

VI.A. One Dimensional Prototype

A scaled down one dimensional version of the STEP system was constructed as a test-bed to ensure the functionality of system components and verify the results of the system simulation. The completed test-bed is shown in Figure VI.1.

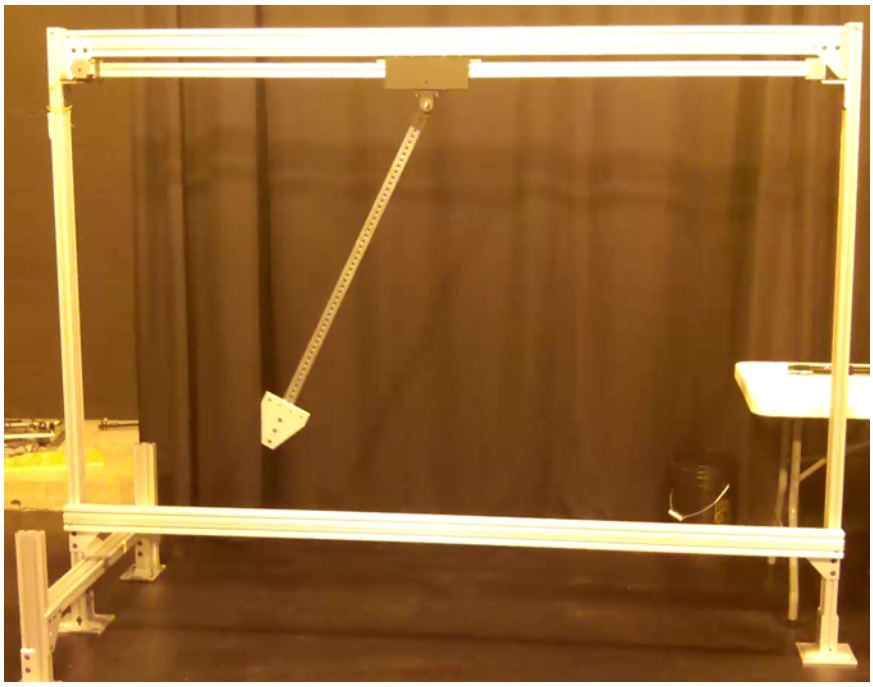

Figure VI.1: One Dimensional STEP Prototype

VI.B. Full System

The STEP system was constructed and is currently suspended from a test stand built of 80/20 aluminum extrusions for testing and for hardware verification and validation. The current version only has a 2.5 meter pendulum, because the test stand does not provide enough height to accommodate the planned 4 meter length. Figures VI.2 through VI.4 show the hardware realizations of the components illustrated in the CAD designs above.

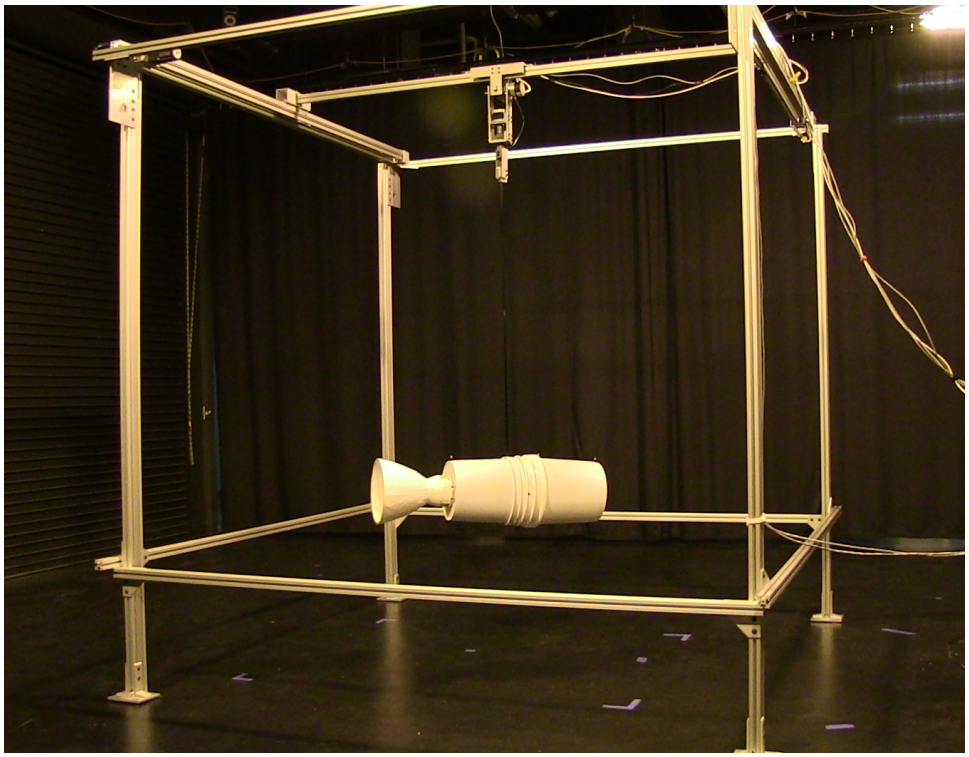

Figure VI.2: Dynamic Payload Pendulum Full View

A simple target vehicle was constructed for use with the Dynamic Payload Pendulum and has been mounted at the base of the carbon fiber rod. This target

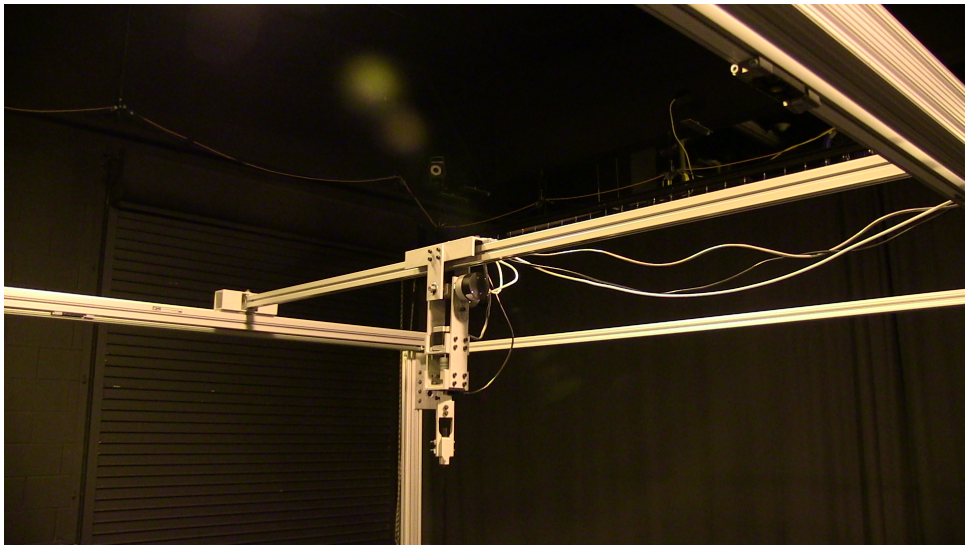

Figure VI.3: Dynamic Payload Pendulum Actuator

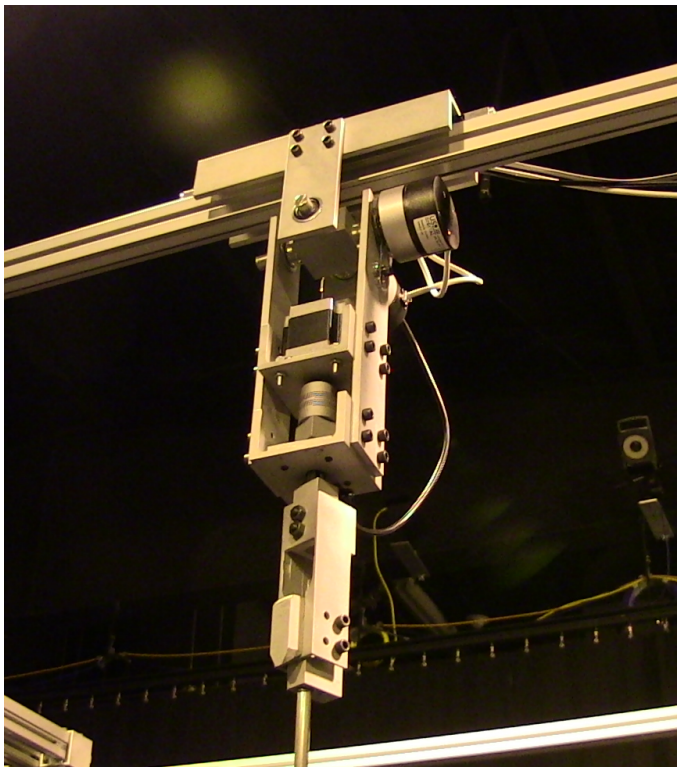

Figure VI.4: Dynamic Payload Pendulum Mount

does not have the capabilities of the target described in section I.B and was simply used for initial system testing. The target used for these initial testing procedures is shown in Figure VI.5.

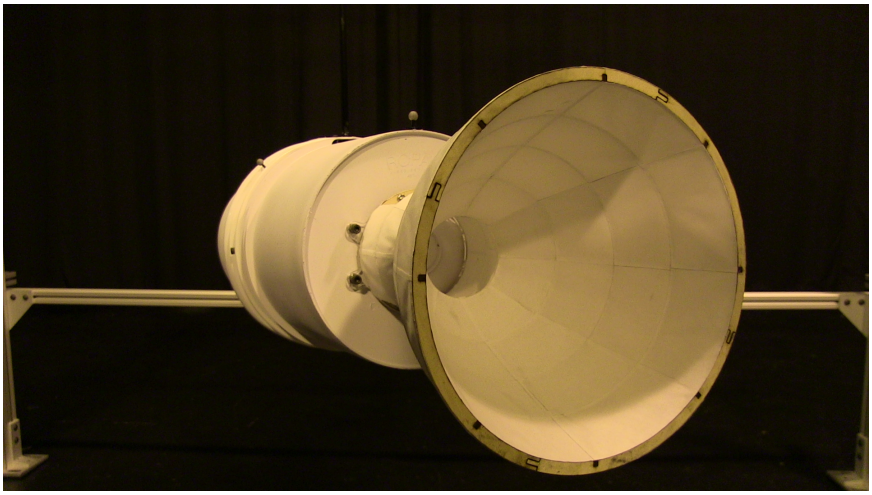

Figure VI.5: Simple Mock Target

VI.C. Control System Electronics

VI.C.1. One Dimensional Prototype

The control system electronics for the one dimensional prototype consisted of a ATMega328™micro-controller that handled communication with the sensors, control computation, and motor control. The stepper motor was driven by a stepper driver board using an Allegro™A4988 stepper driver chip.

VI.C.2. Full System

For the full system a Versalogic Cobra EBX-12 served as the main computer. It managed the communication with the sensor systems and control computation, it then passed the computed controls to the micro-controllers that run both the spin and gantry drive motors. The main computer communicates over USB with an ATMega32U4™micro-controller that controls the spin motor using a stepper driver board with an Allegro™A4988. The main computer also communicates over serial to a ATMega328™micro-controller which was initially intended to control both of the gantry drive motors. The drive stepper motors were to be driven by a pair of driver boards using the Toshiba™TB6560 stepper motor driver chips. However, durring system stesting it was determined that the ATMega328™micro-controller only had the computing capability to control a single axis of the gantry. The electronics setup for the full STEP system is shown in Figure VI.6.

VI.D. Programming

VI.D.1. One Dimensional Prototype

The program architecture for the single degree of freedom prototype consisted of a serial program running on the ATMega328™micro-controller.

VI.D.2. Full System

Initially a serial implementation was attempted for the full STEP system, however it failed due to the system latency it caused, so a parallel architecture was written

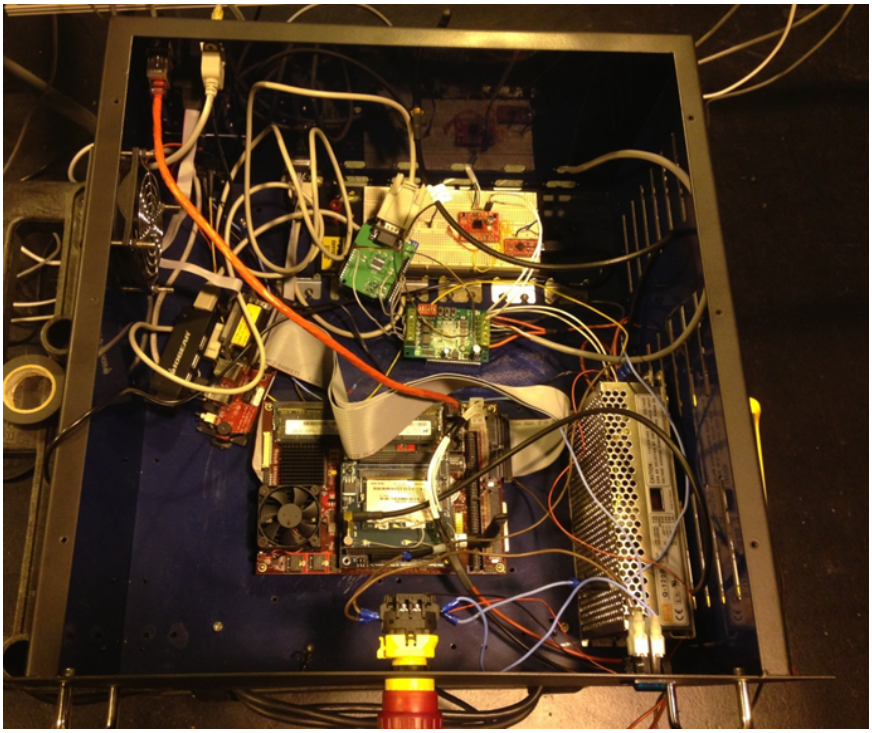

Figure VI.6: Full STEP System Electronics

and implemented. The first component of this implementation consisted of a main control loop running on the main computer at 100 Hertz which preforms the control computation and communicates with the drive and spin motor controllers. There are also two sensor processes on the main computer that handle communication with the encoders and the VN-100. Both of these sensor processes run at 200 Hertz. The final component of this implementation was the motor control loop running on the ATMega328™and ATMega32U4™. To function properly at the highest velocity the motor control loop must run at over 1000 Hertz.

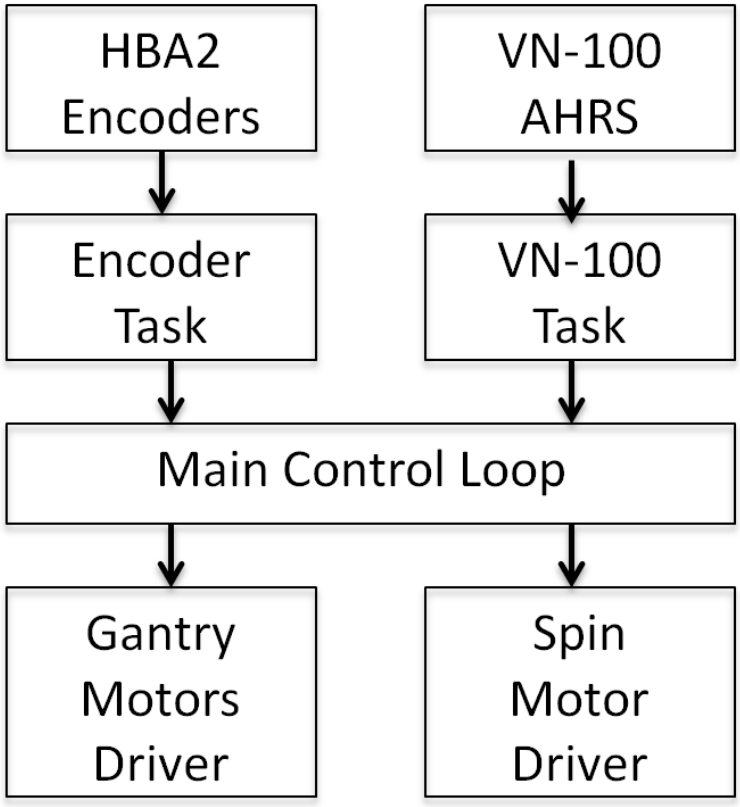

Figure VI.7: Sull STEP System Program Structure

CHAPTER VII

EXPERIMENTAL RESULTS

VII.A. One Dimensional Prototype

After gains with satisfactory performance were identified using the simulation, the controller was implemented on the 1-DOF version of the STEP system. A comparison of experimental results from the 1-DOF version of the STEP taken using the Vicon™motion capture system and the 1-DOF simulation are shown in VII.1. These results illustrate that the simulation provides an extremely good estimate of the one degree of freedom STEP system performance.

VII.B. Full System

As a result of the motor control difficulties described in VI.D, the stabilization controller for the full STEP system was only able to be implemented for a single axis. An experiment was preformed and data was captured with the Vicon™motion capture system. The simulation from V.C was modified to reflect the characteristics of the prototype STEP system as described in VI.B. The x and z axis displacement for both the experiment and the modified full system simulation are shown in Figure VII.2. The results show agreement within centimeters and validate the full STEP system

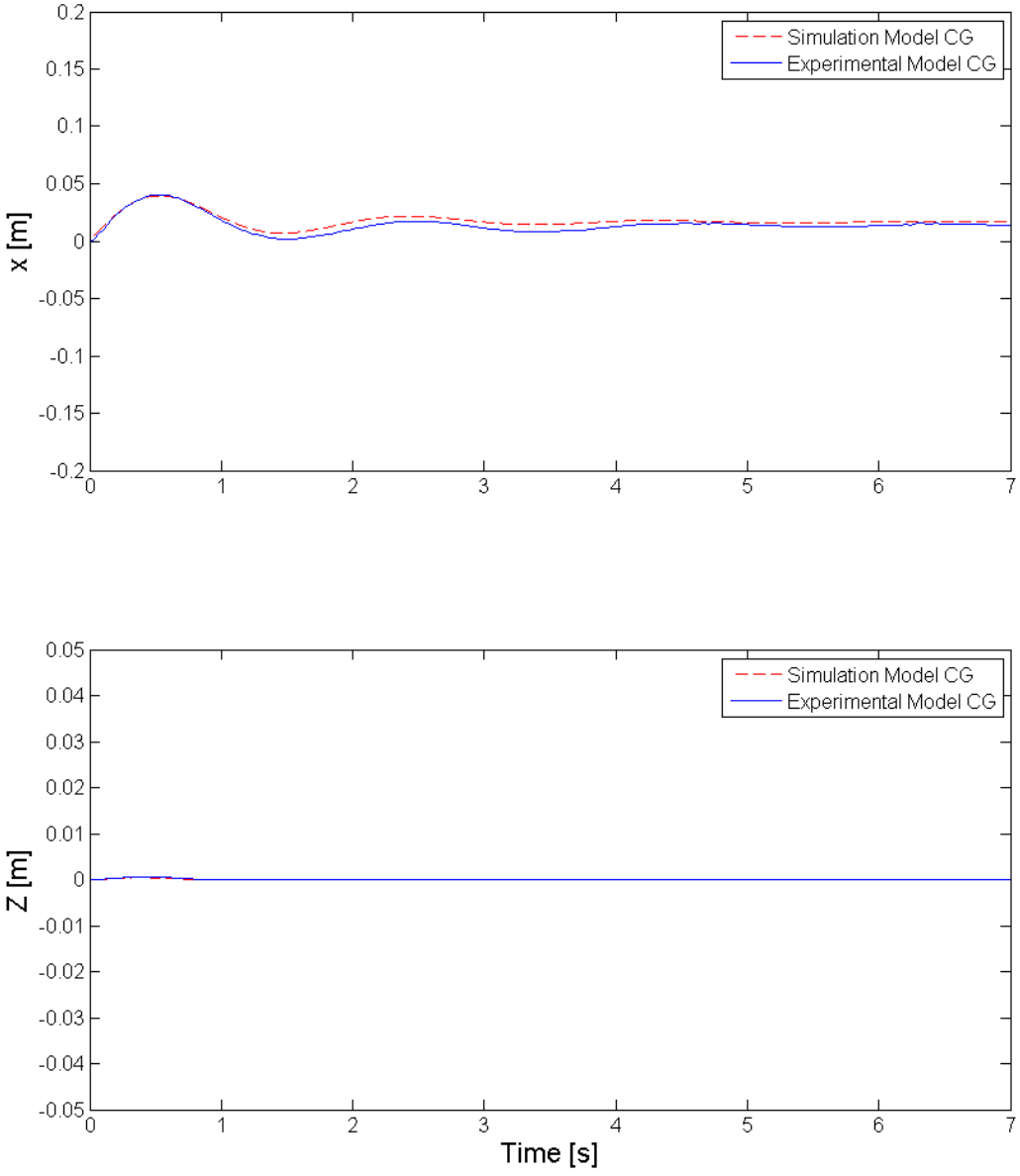

Figure VII.1: 1-DOF Simulated Controller vs. Actual Performance

simulation. The velocity used in this simulation is higher than what the system would normally experience during an actual experiment to illustrate the effectiveness of the controller.

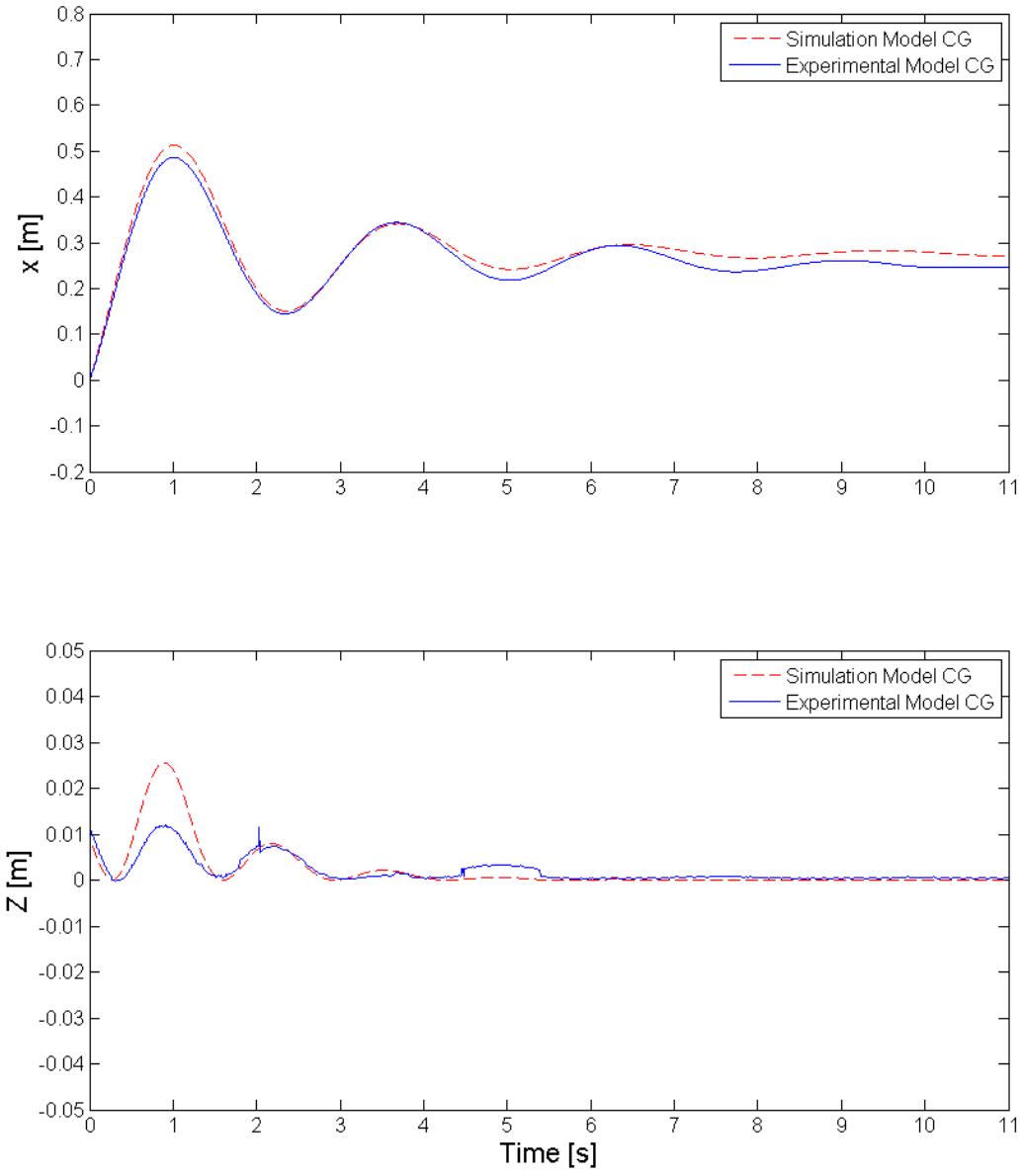

Figure VII.2: Full System Simulation vs. Actual Performance

CHAPTER VIII

CONCLUSION

VIII.A. Summary

The Suspended Target Emulation Pendulum was conceived to allow emulating contact dynamics to the robotics spacecraft proximity operations simulation experiments at the Texas A&M Land, Air, and Space Robotics Laboratory. This capability is important for potential future experiments involving space missions including orbital debris capture, satellite repair, and spacecraft rendezvous and docking. Once fully completed, the STEP system will open up a new avenue for experimentation at the LASR Lab and will hopefully contribute to the development of future space missions.

As demonstrated in Chapters III through VI the design, simulation, and construction of both a single degree of freedom test-bed and an initial iteration of the STEP system have been completed. The only issue encountered was that the current hardware design would require the addition of a second micro-controller for the successful control of both gantry drive axes.

The stabilization controller has been implemented on both the one degree-of-freedom prototype and the one functioning axis of the full system, with the results shown in Chapter VII. The testing of this controller demonstrates the feasibility of the STEP system concept. The agreement with the simulations from Chapter IV

also validates the results that they produce. This indicates that the components of the STEP system control not yet implemented should preform as desired.

VIII.B. Future Work

VIII.B.1. System Upgrade

Support has been secured for the further development of the STEP system. The first step in this process is to upgrade system motors. Stepper motors were chosen because they would produce the required torque at a low price point, however they only allow for velocity level control and are somewhat lacking in their low speed performance. To address these issues the gantry drive motors will be replaced with three Animatics™2315DT SmartMotors with a 4:1 gearbox. These motors have better low speed performance, they will allow for the use of more advanced controllers, and they also have built-in encoders which will provide better accuracy. The spin motor will also be replaced with an Animatics™2315DT. This motor has a lower rotor inertia than the current spin motor and will preform better during the free response component of future experiments.

After these upgrades have been made both the velocity maintenance and stabilization controllers will be implemented on the upgraded system. Additionally, the addition of a form of z-axis actuation and free response is being considered. The free response would be achieved using a constant pressure pneumatic cylinder. Once these upgrades and additions are made the system will be installed in the ceiling at LASR with a full length pendulum arm. System identification studies will then be undertaken to recover the difficult to model characteristics, such as damping and latency. These

studies will then be used to improve the system model in order too achieve better agreement with the experimental results.

VIII.B.2. Mock Target Integration

Once the STEP system is completed we will begin the integration of the advanced mock target vehicles. These mock targets will have the pitch and roll free response capabilities described in I.B. These vehicles will also have precisely defined mass and inertial characteristics that represent a scaled version of actual defunct second stage rocket boosters.

VIII.B.3. Future Experiments

After the mock target integration the STEP system along with the HOMER system will be used for rocket booster capture experiments. These experiments will be used as validation for the control methodologies and capture systems for future missions to capture and deorbit these boosters to address the orbital debris threat. Eventually, the STEP system will be used for experiments representing the other mission types described in I.A.

BIBLIOGRAPHY

[1] Davis, J., Doebbler, J., Daugherty, K., Junkins, J., and Valasek, J., "Aerospace Vehicle Motion Emulation Using Omnidirectional Mobile Platform," *The Proceedings of the AIAA Guidance, Navigation and Control Conference*, 2007.

[2] Shaub, H. and Junkins, J., *Analytical Mechanics of Space Systems*, American Institute of Aeronautics and Astronautics, Reston, VA, 2009.

[3] Hurtado, J., *Kinematic and Kinetic Principles*, Lulu Press, Inc., Raleigh, N.C.

[4] Macron Dynamics Inc., 100 Phyllis Drive, Croydon, Pennsylvania 19021 USA, *MSA-NBC Actuator*, 2013, http://www.macrondynamics.com/belt-actuator/msa-nbc.

[5] Automation Direct, 3505 Hutchinson Road, Cumming, Georgia 30040 USA, *SureStep Stepping Motors*, 2013, Rev: e16-14.

[6] Sparkfun Electronics, 6175 Longbow Dr, Boulder, Colorado 80301 USA, *Stepper Motor - 125 oz.in (200 steps/rev)*, 2013, https://www.sparkfun.com/products/10847.

[7] US Digital, 1400 NE 136th Avenue, Vancouver, Washington 98684 USA, *HBA2 Absolute Blind Hollow Bore Optical Encoder*, 2012, Rev: 130731113215.

[8] VectorNav Technologies, 903 N Bowser Rd., Suite 200, Richardson, Texas 75081 USA, *VN -100 User Manual*, 2013, Rev: 1.2.10.

[9] Hurtado, J., *Elements of Spacecraft Control*, Lulu Press, Inc., Raleigh, N.C.

[10] "Wang, X., Schmitt, C., and Payne, M., "Oscillations with Three Damping Effects," *European Journal Of Physics*, Vol. 23(2), 2002.